Nuclear Inst. and Methods in Physics Research, A 1045 (2023) 167551

Contents lists available at ScienceDirect

Nuclear Inst. and Methods in Physics Research, A

journal homepage: www.elsevier.com/locate/nima

Neutron capture of UO_2 targets prepared by spin-coating assisted combustion synthesis

Ashabari Majumdar [a], Khachatur V. Manukyan [a,*], Wanpeng Tan [a], Stefania Dede [a,b], Jordan M. Roach [c], Aaron Couture [d], Peter C. Burns [c,e], Ani Aprahamian [a,f]

[a] Nuclear Science Laboratory, Department of Physics, University of Notre Dame, Notre Dame, IN 46556, USA
[b] Cyclotron Institute, Texas A&M University, College Station, TX 77843, USA
[c] Department of Chemistry and Biochemistry, University of Notre Dame, Notre Dame, IN 46556, USA
[d] Physics Division, Los Alamos National Laboratory, Los Alamos, NM 87545, USA
[e] Department of Civil and Environmental Engineering and Earth Sciences, University of Notre Dame, Notre Dame, IN 46556, USA
[f] A. Alikhanyan National Science Laboratory of Armenia, 2 Alikhanyan Brothers, 0036 Yerevan, Armenia

ARTICLE INFO

Keywords:
Actinide targets
Uranium dioxide
Solution combustion synthesis
Neutron capture

ABSTRACT

Two uranium dioxide (UO_2) targets of (414 ± 23) nm and (1092 ± 93) nm thicknesses were prepared on 6061 aluminum alloy and puratronic grade aluminum backing materials. The targets were deposited with a novel method combining spin coating and solution combustion synthesis (SCS). The target layers consisted of small (3–7 nm) UO_2 grains and uniformly distributed ultra-small (1–3 nm) pores. The prepared targets were tested at the Los Alamos National Laboratory's LANSCE facility for neutron irradiation damage and suitability for neutron capture experiments. The samples showed no signs of target material loss after the irradiation. However, irradiation caused a significant increase in the grain size (4–10 nm), as well as upward mass diffusion and coalescence of the pores due to the thermal spikes. The magnesium in the aluminum 6061 alloy backing also diffused into the UO_2 layer during neutron irradiation. The structural changes in the target after the irradiation do not affect the data from neutron capture. The new method can be used more broadly to prepare other actinide targets for nuclear physics experiments.

1. Introduction

Thin actinide targets are of great interest for a variety of needs, from better quantification of advanced nuclear fuel cycles to stockpile stewardship programs and from nuclear astrophysics to nuclear structure studies [1–4]. One of the sources of uncertainties in measurements involving actinides is the precise determination of the thicknesses, uniformity, and robustness of the targets in experiments. The existing target preparation techniques have considerable limitations. For example, the neutron capture measurements of ^{238}U reported by Ullmann et al. utilized depleted uranium foils and enriched uranium oxide targets electrodeposited on a thin titanium backing [5]. The preparation of metallic foils requires significant initial processing (mechanical rolling), posing safety hazards associated with using pyrophoric uranium. Electrodeposition and molecular plating methods are more straightforward; however, the targets are often inhomogeneous and contain impurities [6–9]. Also, the target layers generally have low adherence to the backings, thereby reducing the mechanical integrity of the targets during experiments.

Casperson et al. [10] used a high vacuum evaporation method to prepare thin (100 μg/cm^2) ^{238}U and ^{235}U targets for neutron capture cross-section measurements. Despite the high uniformity of vacuum-deposited targets, the material collection efficiency for this method is low (10%–30%). The loss of expensive and sometimes highly radioactive isotopically enriched materials limits the application of this method. Also, it is challenging to prepare relatively thicker (above 200 μg/cm^2) targets by vacuum deposition.

Recently, we reported on simple procedures to prepare thin uranium oxide targets [11,12]. The process involves depositing a thin layer of *uranyl nitrate-acetylacetone-2-methoxyethanol* or *uranyl nitrate-glycine-water* solutions on a backing, followed by short (20 min) annealing at a temperature range of 350–400 °C. The annealing results in the combustion of the solution layers, creating thin (35–50 nm) and uniform films of UO_2. The use of multiple deposition cycles allowed us to produce targets with thicknesses up to ~300 nm. The targets prepared by these approaches are highly robust when irradiated with high-energy (1.7 MeV) Ar^{2+} ions of up to 1×10^{17} ions/cm^2. X-ray fluorescence (XRF) measurements and alpha-particle spectroscopy showed that the targets did not undergo degradation.

This article reports on the preparation of thicker (up to 1100 nm) UO_2 targets (depleted uranium) on two different aluminum backings

* Corresponding author.
E-mail address: kmanukya@nd.edu (K.V. Manukyan).

https://doi.org/10.1016/j.nima.2022.167551
Received 26 June 2022; Received in revised form 20 September 2022; Accepted 27 September 2022
Available online 10 October 2022

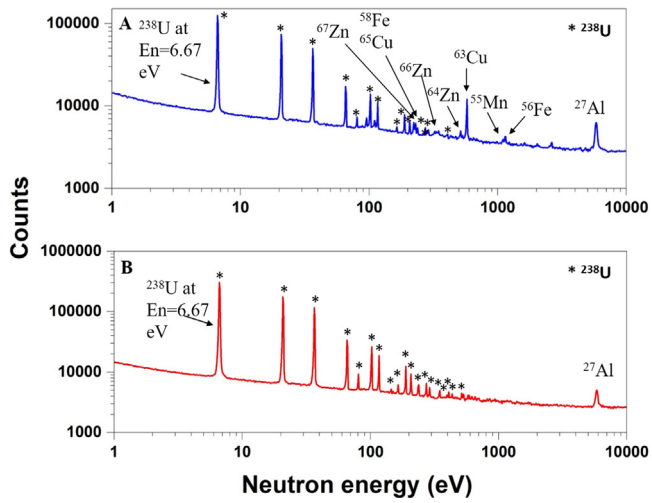

Fig. 1. Neutron capture spectra from Target-1 (A) and Target-2 (B) showing the neutron capture peaks from ^{238}U (labeled with*) and the backing elements peaks (labeled).

utilizing the spin coating-assisted solution combustion synthesis (SCS) method. These targets were tested for robustness under neutron irradiation at the Los Alamos Neutron Science Center (LANSCE) of the Los Alamos National Laboratory. We characterized the targets before and after exposure to the neutron beam by an array of high-resolution electron microscopy, diffraction methods, and alpha-particle spectroscopy. While the targets were robust through the experiment showing no sign of degradation, the characterization of the neutron-irradiated targets revealed structural and compositional changes at the nanoscale level.

2. Experimental method and data analysis

Two depleted UO_2 targets were prepared using spin-coating assisted SCS. The target preparation method is reported in our previous work [11]. Briefly, to prepare the first target (**Target-1**), 100 μL of uranyl nitrate-acetylacetone-2-methoxyethanol solution was pipetted on a mirror finished Al 6061 alloy (McMaster-Carr) disc with 41.4 mm diameter and 0.25 mm thickness while rotating it at a speed of 3000 rpm for 35 s. This 6061 alloy backing contains the following additives: Mg (~1%), Si (~0.6%) Fe (~0.7%), Cu (~0.25%), Cr (~0.15%), Zn (~0.25%), Mn (~0.15%), and Ti (~0.15%) by weight. After the deposition of the solution, the material was placed in a pre-heated (400 °C) furnace for 15 min. The process was repeated 13 times. The second target (**Target-2)** was made with the same solution and coating parameters but the process was repeated for 30 deposition cycles on a puratronic grade aluminum (99.997%, Alpha Aesar) backing. The active areas of both targets were circular region with a 20 mm diameter at the center of the backings.

The neutrons were produced by spallation reactions of 800 MeV protons (100 μA) impinging on tungsten targets at LANSCE. The proton pulses are 125 ns full width at half maxima with a frequency of 20 Hz [13]. The neutron flux follows a $1/E_n$ curve and has the value of 1.5×10^4 neutrons per energy decade per proton pulse within the neutron energy range from 1 eV to 1 MeV at the sample site [14]. The neutron beam diameter was ~10 mm. Targets 1 and 2 were irradiated with neutrons for 22 and 29 h to deposit a total fluence of 2.3×10^{11} and 3.0×10^{11} neutrons/cm^2, respectively. The Detector for Advanced Neutron Capture Experiments (DANCE) array, consisting of 160 barium fluoride crystals, was utilized to detect γ rays emitted during the capture.

A Titan 80–300 (FEI) transmission electron microscope (TEM) was used to investigate the morphology, composition, and crystallinity of pristine and neutron-irradiated targets. An electron dispersive X-ray spectroscopy (EDS, Oxford Inca) system with a Si-Li detector (energy resolution of ~130 eV at 5.9 keV) installed within the microscope is used for elemental analysis. A Helios Nanolab 600 (Thermo Fisher Scientific) dual electron/ion beam system was employed to produce cross-sectional thin (50–100 nm) samples for TEM analysis [15]. An Orbis XRF analyzer consisting of a Rh X-ray tube, poly-capillary optics, and an 80 mm^2 Si (Li) drift detector is used to determine the elemental composition of the targets at the millimeter scale. The α particles emitted from the targets were counted with an Alpha Suite Spectrometer (ORTEC-ULTRA-AS) at ~10 Pa pressure using an ion-implanted silicon detector (active area: - 900 mm^2, resolution: - 29 keV at 5.486 MeV). These measurements were used to determine the number of each uranium isotope per cm^2 target area before and after irradiation. For this purpose, the effects of detector geometry, the energy loss of α-particles before reaching the detector, and the branching ratio were considered. The detailed description of the α particle spectroscopy analysis procedure followed is described in our previous work [11].

3. Results and discussion

The thicknesses or areal densities of the targets measured from cross-sectional TEM images were (414 ± 23) nm/ (454 ± 26) μg/cm^2 for Target-1 and (1092 ± 93) nm/ (1199 ± 102) μg/cm^2 for Target-2. Table 1 shows the uranium isotopic composition of pristine targets measured by α-particle spectroscopy. Table 1 also shows that the number of each isotope in the targets did not change significantly after the neutron capture experiment, indicating that targets are robust and do not undergo any significant degradation. The robustness of the uranium content in the targets was also confirmed using XRF analysis by measuring the intensity of the characteristic U Lα line at multiple locations on both targets before and after irradiation. The ratio of the U Lα line is ~1 for both targets (Supplementary Information, Table S1), consistent with the results of α-spectroscopy.

The robustness of the targets was confirmed by analyzing the capture yield during the neutron irradiation experiment as well. Fig. 1 shows the neutron capture yield spectrum obtained for Target-1 (Panel A) and Target-2 (Panel B) for the neutron energy range of 1–10,000 eV. The details of the neutron capture peaks by the targets and the backings are shown in Table S2.

Neutron capture on ^{238}U has a Q value of 4.8 MeV (Figure S1), which is used to isolate the ^{238}U capture signature. The spectrum for Target-1 also exhibits peaks for neutron capture reactions on the isotopes present in the backing Al 6061 alloy (^{27}Al, ^{55}Mn, ^{56}Fe, ^{58}Fe, ^{63}Cu, ^{65}Cu, ^{64}Zn, ^{66}Zn, and ^{67}Zn). However, peaks from neutron capture on some of the additives present in Al 6061 (Si, Mg, Cr, and Ti) are not seen. Si, Mg, and Cr have low neutron cross-sections compared to the rest of the isotopes detected. Although Ti has a significant neutron

Table 1
The nuclei number per cm^2 of each isotope present in pristine and irradiated targets measured by α particle spectroscopy.

	Target 1		Target 2	
	Pristine	Irradiated	Pristine	Irradiated
^{238}U	(4.20 ± 0.16)E+18	(4.27 ± 0.17)E+18	(8.96 ± 0.34)E+18	(9.44 ± 0.37)E+18
^{235}U	(1.19 ± 0.47)E+16	(1.25 ± 0.45)E+16	(2.35 ± 0.15)E+16	(2.49 ± 0.20)E+16
^{236}U	(2.00 ± 0.14)E+14	(2.07 ± 0.14)E+14	(4.72 ± 0.40)E+14	(5.11 ± 0.31)E+14
^{234}U	(3.08 ± 0.37)E+13	(3.09 ± 0.35)E+13	(6.36 ± 0.11)E+13	(6.09 ± 0.14)E+13

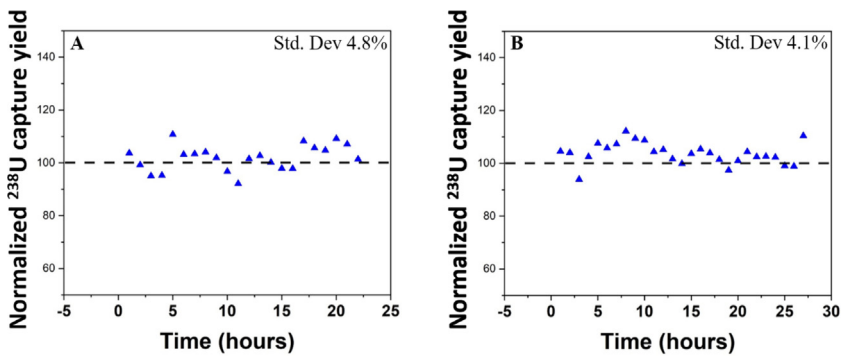

Fig. 2. Normalized neutron capture yield from the ^{238}U peak at neutron energy of 6.67 eV is shown for each hour of 22 and 29 h long runs for Target-1 (A) and Target-2 (B) respectively.

capture cross-section, the abundance of this isotope in the alloy backing is low (0.15%). Target 2 shows peaks resulted from neutron capture on ^{238}U and ^{27}Al.

We selected the most prominent peak at E_n = 6.67 eV for ^{238}U (Fig. 1) to evaluate the target robustness [16]. Using appropriate Q value (3.25–5.25 MeV) and neutron energy (E_n = 5.5–7.5 eV) gates, yields obtained from ^{238}U neutron capture for each hour-long run are determined. These yields are normalized using the total charge of the proton beam. Fig. 2 shows that the yield stays reasonably constant throughout the irradiation. The uncertainty of the method can be inferred from the standard deviation of the capture yield, which is 4.8% for Target-1 and 4.1% for Target-2. Fig. 2 shows no specific pattern in the data, such as a steady decline of the counts during the experiment, further reinforcing the initial determination of the high robustness of the targets.

Small samples (5 × 5 × 0.07 μm^3) lifted from the targets were imaged with the high-angle annular dark-field (HAADF) scanning TEM method. From these images, the UO_2 layers before irradiation are found to be smooth (Fig. 3). Each deposited layer is ~32 nm for Target-1 and ~36 nm for Target-2. All the layers were found to be uniform throughout the entire target thickness. Imaging the irradiated Target-1 revealed the emergence of 5–10 nm pores relatively uniformly distributed throughout the UO_2 target. The near-surface layer of this target also contains a few larger (10–15 nm) pores. Fig. 3 reveals that the near-surface layer of the irradiated Target-2 exhibits significantly larger (20–25 nm) pores. Close to the target/backing interface, the UO_2 exhibits much less porosity than the surface for both irradiated samples. Exposure to high-energy neutron beams is known to cause swelling, bubbling, and formation of pores in UO_2 due to the release of fission gas products [17,18]. However, the neutron capture experiment in this work is performed primarily at energies below the fission threshold. Therefore, the origin of the morphological changes in our targets must be due to a different effect.

To reveal the irradiation effect on grain-scale restructuring, we use high-resolution TEM imaging for near-surface layers of Target-1. A TEM image of the pristine target displays grains with lattice fringes from the (111) and (220) planes (Fig. 4A, left panel). The grain diameter ranges from 2.5 to 6.5 nm, with an average value of 4.3 nm (Fig. 4A, center). The radially averaged intensity distribution profile as a function of the scattering vector obtained from the selected electron diffraction (SAED) pattern displays broad diffraction peaks (right panel on Fig. 4A). These peaks are aligned well with diffraction lines for the calculated UO_2 pattern. Several adjacent diffraction peaks, such as (111) and (200) or (220), (311), and (222), are not well resolved due to the ultra-small sizes of the grains. The neutron irradiation considerably increases grain sizes making them more *polydisperse,* ranging from *3.5 to 9.5 nm with* an average of ~6.7 nm (Fig. 4B). The SAED pattern and diffraction profiles display noticeable changes related to the grain coarsening. For example, the (220), (311), and (222) reflections become significantly narrower and well resolved (right panel on Fig. 4B).

We also conducted TEM/SAED measurements on samples taken from the irradiated Target-2 (Fig. 5). TEM images of the near-surface layers and the target/backing interface show grains with lattice fringes from (111) and (220) planes. The grain sizes on the surface range from 3 to 6 nm, while at the interface, they are slightly smaller (2.5–5 nm). For the near-surface layer, diffraction peaks are narrower and better resolved than those at the interface.

The pristine targets prepared by SCS have small (1–3 nm) pores uniformly distributed throughout the UO_2 layers. Although there is no target heating at macroscopic scales during irradiation, each neutron capture reaction or scattering event can deposit energy resulting in thermal spikes within the grain containing the given target atom. Due to small grain sizes, this process of thermal spikes could propagate across grain boundaries facilitating rapid atomic migration (mass diffusion), new grain nucleation, and growth. The diffusion depends on the atomic mobility at the given irradiation temperature. The grain growth is more pronounced on the surface than in the inner layers due to the unequal heat deposition along the target thickness, i.e., the deposited heat is higher on the surface and decreases along the target thickness. We can suggest that irradiation-induced clustering on the surface is promoted by the lower steric hindrance (higher mobility of atoms). Within the target layers, the material has to overcome a higher energy barrier to diffuse and re-organize, forming clusters. For both targets, the grain growth is confirmed by the TEM image (Figs. 4 and 5). However, grain growth is more pronounced for Target-1.

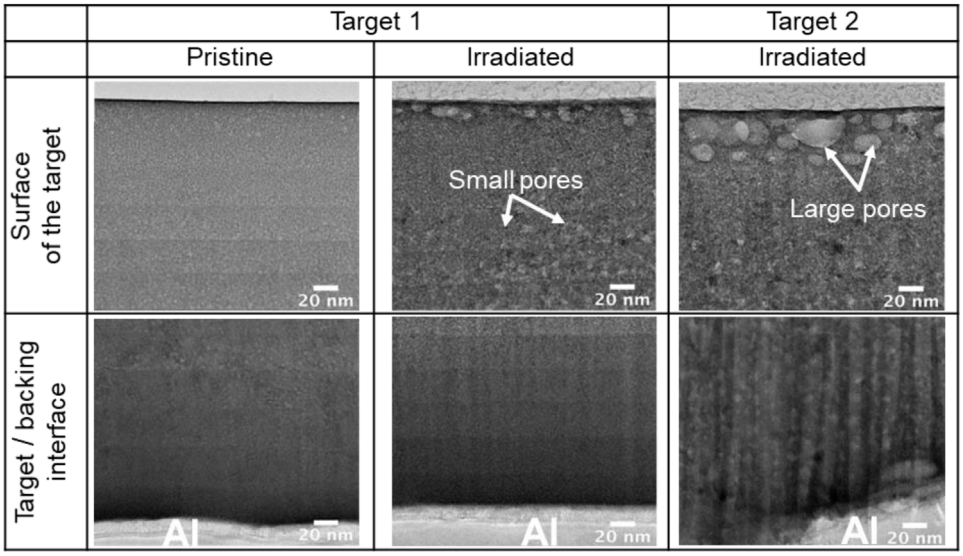

Fig. 3. HAADF scanning TEM images of the pristine neutron-irradiated targets.

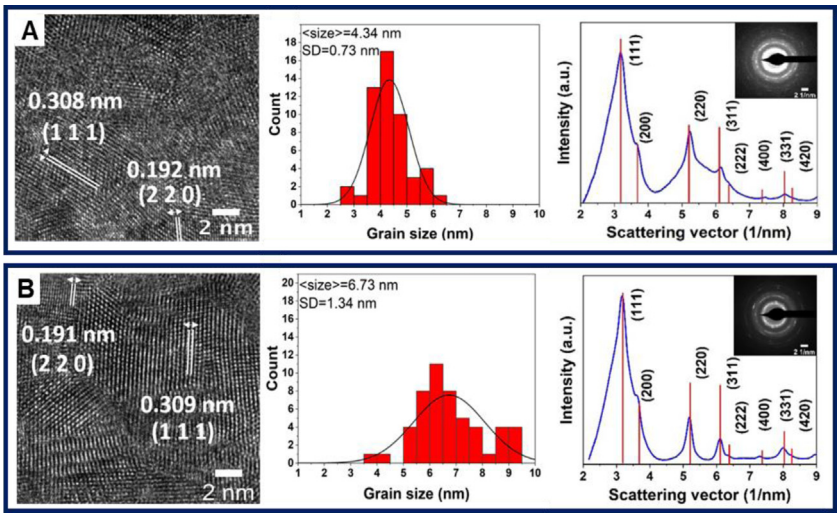

Fig. 4. High-resolution TEM images (left), grain size distribution (center), and selected area electron diffraction patterns and profiles (right) for pristine (A) and irradiated (B) Target-1.

We also conducted EDS elemental mapping to reveal the origin of different grain growth. These analyses show that uranium and oxygen are uniformly distributed in the target layers before and after irradiation (Figure S2). However, the distribution of Mg for Target-1 deposited on the Al 6061 alloy backing shows an interesting pattern. Fig. 6A illustrates that the pristine Target-1 exhibits an increased concentration of Mg at and near the target/backing interface. Fig. 6B indicates that irradiation increases the Mg concentration in the UO_2. The point-by-point EDS analysis confirms that the Mg diffuses from the backing into the target layer during irradiation (Fig. 6C). These results show that the multiple target deposition and heat treatment cycles selectively leach the Mg from the Al 6061 alloy backing even though the Mg is mainly confined to the target/backing interface. Compared to the pristine target, neutron irradiation facilitates further diffusion of Mg and incorporation into the target layers. EDS analysis for Target-2 deposited on high-purity Al does not show the presence of Mg. The small amount of Mg could accelerate mass diffusion and facilitate grain growth in Target-1.

4. Conclusion

This work shows that spin coating-assisted SCS allows the preparation of relatively thick (up to ~1100 nm or 1.2 mg/cm^2), robust, and uniform uranium dioxide targets. This method will be extended to make more exotic and isotopically pure targets required for fundamental science research and applications. The two depleted UO_2 targets of varying thicknesses and backings were prepared at the University of Notre Dame and tested by neutron irradiation at the LANSCE facility of the Los Alamos National Laboratory. The targets remained robust under neutron beam irradiation and showed no material loss throughout the experiment as monitored by capture yield. The robustness of the targets was further confirmed with offline analysis using XRF and α-particle spectroscopy. Electron microscopy investigations before irradiation exhibited that the targets have small grains (3–6 nm) and ultra-small pores (1–3 nm). After irradiation, these pores became significantly larger (20–25 nm), primarily located at the near-surface layers. The

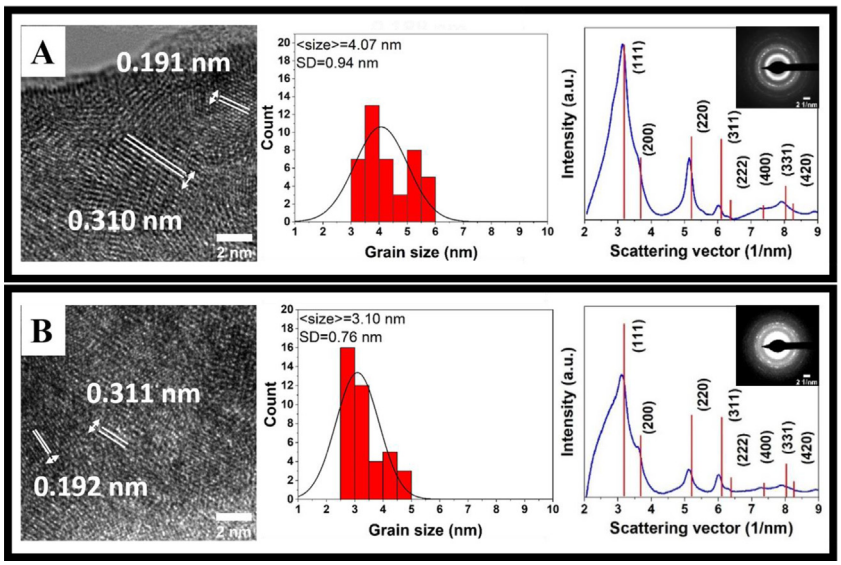

Fig. 5. High-resolution TEM images (left), grain size distribution (center) and selected area electron diffraction patterns and profiles (right) for irradiated Target-2 near-surface (A) and UO_2/Al interface areas (B).

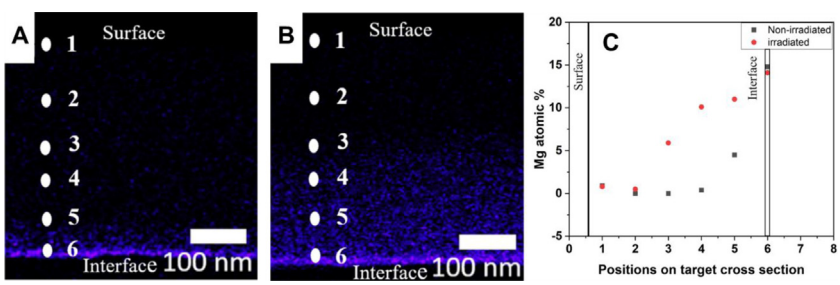

Fig. 6. EDS elemental mapping of the Mg K line in Target-1 before (A) and after (B) irradiation and point-by-point Mg content in the UO_2 layer (C).

beam-induced thermal spikes likely cause mass diffusion, grain nucleation, and growth. The backings also influence the composition of the targets upon irradiation.

Declaration of competing interest

The authors declare that they have no known competing financial interests or personal relationships that could have appeared to influence the work reported in this paper.

Data availability

No data was used for the research described in the article.

Acknowledgments

The work was performed with financial support from the U.S. Department of Energy's (DOE) National Nuclear Security Administration, USA (NNSA, Grants # DE-NA0003888, and NA0004093), U.S. National Science Foundation (NSF, PHY 2011890), and JINA-CEE Physics Frontiers Center, USA (Award #1430152). A.A. acknowledges support from the Fulbright U.S. Scholar grant. K.M. also acknowledges funding from the U.S. Army Research Office Grant # W911NF2110045 under the Materials Synthesis & Processing Program, with Dr. Michael P. Bakas as the program manager. This research benefited from the use of LANSCE, which is supported by the NNSA, USA under Contract No. 89233218CNA000001. A. C. was supported by the DOE, USA through the LANL. LANL is operated by Triad National Security, LLC, for the NNSA of U.S. DOE (Contract No. 89233218CNA000001). The authors also acknowledge Notre Dame Center for Environmental Science & Technology (CEST) and Integrated Imaging Facility (NDIIF) for instrumental usage.

Appendix A. Supplementary data

Supplementary material related to this article can be found online at https://doi.org/10.1016/j.nima.2022.167551.

References

[1] M.B. Chadwick, M. Herman, P. Obložinský, M.E. Dunn, Y. Danon, A.C. Kahler, D.L. Smith, B. Pritychenko, G. Arbanas, R. Arcilla, R. Brewer, D.A. Brown, R. Capote, A.D. Carlson, Y.S. Cho, H. Derrien, K. Guber, G.M. Hale, S. Hoblit, S. Holloway, T.D. Johnson, T. Kawano, B.C. Kiedrowski, H. Kim, S. Kunieda, N.M. Larson, L. Leal, J.P. Lestone, R.C. Little, E.A. McCutchan, R.E. MacFarlane, M. MacInnes, C.M. Mattoon, R.D. McKnight, S.F. Mughabghab, G.P.A. Nobre, G. Palmiotti, A. Palumbo, M.T. Pigni, V.G. Pronyaev, R.O. Sayer, A.A. Sonzogni, N.C. Summers, P. Talou, I.J. Thompson, A. Trkov, R.L. Vogt, S.C. van der Marck, A. Wallner, M.C. White, D. Wiarda, P.G. Young, ENDF/B-VII.1 nuclear data for science and technology: Cross sections, covariances, fission product yields and decay data, Nucl. Data Sheets. 112 (2011) 2887–2996, http://dx.doi.org/10.1016/j.nds.2011.11.002.

[2] J.D. Baker, C.A. McGrath, T.S. Hill, R. Reifarth, F. Tovesson, Actinide targets for neutron cross section measurements, J. Radioanal. Nucl. Chem. 276 (2008) 555–560, http://dx.doi.org/10.1007/s10967-008-0541-x.

[3] J.J. Hecla, A. Danagoulian, Nuclear disarmament verification via resonant phenomena, Nature Commun. 9 (2018) 1259, http://dx.doi.org/10.1038/s41467-018-03680-4.

[4] M. Jandel, T.A. Bredeweg, E.M. Bond, M.B. Chadwick, R.R. Clement, A. Couture, J.M. O'Donnell, R.C. Haight, T. Kawano, R. Reifarth, R.S. Rundberg, J.L. Ullmann, D.J. Vieira, J.B. Wilhelmy, J.M. Wouters, U. Agvaanluvsan, W.E. Parker, C.Y. Wu, J.A. Becker, Neutron capture cross section of^{241}Am, Phys. Rev. C 78 (2008) 034609, http://dx.doi.org/10.1103/PhysRevC.78.034609.

[5] J.L. Ullmann, T. Kawano, T.A. Bredeweg, A. Couture, R.C. Haight, M. Jandel, J.M. O'Donnell, R.S. Rundberg, D.J. Vieira, J.B. Wilhelmy, J.A. Becker, A. Chyzh, C.Y. Wu, B. Baramsai, G.E. Mitchell, M. Krtika, Cross section and γ -ray spectra for U 238 (n, γ) measured with the DANCE detector array at the Los Alamos Neutron Science Center, Phys. Rev. C 89 (2014) 034603, http://dx.doi.org/10.1103/PhysRevC.89.034603.

[6] S. Sadi, A. Paulenova, P.R. Watson, W. Loveland, Growth and surface morphology of uranium films during molecular plating, Nucl. Instrum. Methods Phys. Res. 655 (2011) 80–84, http://dx.doi.org/10.1016/j.nima.2011.06.025.

[7] W. Parker, H. Bildstein, N. Getoff, Molecular plating I, a rapid and quantitative method for the electrodeposition of thorium and uranium, Nucl. Instrum. Methods. 26 (1964) 55–60, http://dx.doi.org/10.1016/0029-554X(64)90049-7.

[8] A. Vascon, S. Santi, A.A. Isse, A. Kühnle, T. Reich, J. Drebert, K. Eberhardt, C.E. Düllmann, Smooth crack-free targets for nuclear applications produced by molecular plating, Nucl. Instrum. Methods Phys. Res. A 714 (2013) 163–175, http://dx.doi.org/10.1016/j.nima.2013.03.003.

[9] L. Benedik, G. Sibbens, A. Moens, R. Eykens, M. Necemer, S.D. Škapin, P. Kump, Preparation of thick uranium layers on aluminium and stainless steel backings, Appl. Radiat. Isot. 87 (2014) 238–241, http://dx.doi.org/10.1016/j.apradiso.2013.11.052.

[10] R.J. Casperson, D.M. Asner, J. Baker, R.G. Baker, J.S. Barrett, N.S. Bowden, C. Brune, J. Bundgaard, E. Burgett, D.A. Cebra, T. Classen, M. Cunningham, J. Deaven, D.L. Duke, I. Ferguson, J. Gearhart, V. Geppert-Kleinrath, U. Greife, S. Grimes, E. Guardincerri, U. Hager, C. Hagmann, M. Heffner, D. Hensle, N. Hertel, D. Higgins, T. Hill, L.D. Isenhower, J. King, J.L. Klay, N. Kornilov, R. Kudo, A.B. Laptev, W. Loveland, M. Lynch, W.S. Lynn, J.A. Magee, B. Manning, T.N. Massey, C. McGrath, R. Meharchand, M.P. Mendenhall, L. Montoya, N.T. Pickle, H. Qu, J. Ruz, S. Sangiorgio, K.T. Schmitt, B. Seilhan, S. Sharma, L. Snyder, S. Stave, A.C. Tate, G. Tatishvili, R.T. Thornton, F. Tovesson, D.E. Towell, R.S. Towell, N. Walsh, S. Watson, B. Wendt, L. Wood, L. Yao, W. Younes, Measurement of the normalized ^{238}U(n, f)/ ^{235}U (n, f) cross section ratio from threshold to 30 MeV with the NIFFTE fission time projection Chamber, Phys. Rev. C 97 (2018) 034618, http://dx.doi.org/10.1103/PhysRevC.97.034618.

[11] A. Majumdar, K.V. Manukyan, S. Dede, J.M. Roach, D. Robertson, P.C. Burns, A. Aprahamian, Irradiation-driven restructuring of UO_2 thin films: Amorphization and crystallization, ACS Appl. Mater. Interfaces. 13 (2021) 35153–35164, http://dx.doi.org/10.1021/acsami.1c08682.

[12] J.M. Roach, K.V. Manukyan, A. Majumdar, S. Dede, A.G. Oliver, P.C. Burns, A. Aprahamian, Hyperstoichiometric uranium dioxides: Rapid synthesis and irradiation-induced structural changes, Inorg. Chem. 60 (2021) 18938–18949, http://dx.doi.org/10.1021/acs.inorgchem.1c02736.

[13] T.A. Bredeweg, M.M. Fowler, J.A. Becker, E.M. Bond, M.B. Chadwick, R.R.C. Clement, E.I. Esch, T. Ethvignot, T. Granier, M. Jandel, R.A. Macri, J.M. O'Donnell, R. Reifarth, R.S. Rundberg, J.L. Ullmann, D.J. Vieira, J.B. Wilhelmy, J.M. Wouters, C.Y. Wu, Simultaneous measurement of (n, γ) and (n, fission) cross sections with the DANCE 4π BaF2 array, Nucl. Instrum. Methods Phys. Res. B 261 (2007) 986–989, http://dx.doi.org/10.1016/j.nimb.2007.04.226.

[14] R. Reifarth, T.A. Bredeweg, A. Alpizar-Vicente, J.C. Browne, E.I. Esch, U. Greife, R.C. Haight, R. Hatarik, A. Kronenberg, J.M. O'Donnell, R.S. Rundberg, J.L. Ullmann, D.J. Vieira, J.B. Wilhelmy, J.M. Wouters, Background identification and suppression for the measurement of (n, γ) reactions with the DANCE array at LANSCE, Nucl. Instrum. Methods Phys. Res. Sect. A 531 (2004) 530–543, http://dx.doi.org/10.1016/j.nima.2004.05.096.

[15] K. Manukyan, C. Fasano, A. Majumdar, G.F. Peaslee, M. Raddell, E. Stech, M. Wiescher, Surface manipulation techniques of Roman denarii, Appl. Surf. Sci. 493 (2019) 818–828, http://dx.doi.org/10.1016/j.apsusc.2019.06.296.

[16] H.I. Kim, C. Paradela, I. Sirakov, B. Becker, R. Capote, F. Gunsing, G.N. Kim, S. Kopecky, C. Lampoudis, Y.O. Lee, R. Massarczyk, A. Moens, M. Moxon, V.G. Pronyaev, P. Schillebeeckx, R. Wynants, Neutron capture cross section measurements for ^{238}U in the resonance region at GELINA, Eur. Phys. J. A 52 (2016) 170, http://dx.doi.org/10.1140/epja/i2016-16170-6.

[17] J. Rest, M.W.D. Cooper, J. Spino, J.A. Turnbull, P. Van Uffelen, C.T. Walker, Fission gas release from UO_2 nuclear fuel: A review, J. Nucl. Mater. 513 (2019) 310–345, http://dx.doi.org/10.1016/j.jnucmat.2018.08.019.

[18] N. Nakae, Y. Iwata, T. Kirihara, Thermal recovery of defects in neutron irradiated UO_2, J. Nucl. Mater. 80 (1979) 314–322, http://dx.doi.org/10.1016/0022-3115(79)90194-6.